Biochimica et Biophysica Acta 1828 (2013) 1715–1722

Contents lists available at SciVerse ScienceDirect

Biochimica et Biophysica Acta

journal homepage: www.elsevier.com/locate/bbamem

Water influx and cell swelling after nanosecond electropermeabilization

Stefania Romeo [a,b,*], Yu-Hsuan Wu [c], Zachary A. Levine [d], Martin A. Gundersen [c,d,e], P. Thomas Vernier [e]

[a] CNR-Institute for Electromagnetic Sensing of Environment (IREA), via Diocleziano 328, 80124, Naples, Italy
[b] Department of Information Engineering, Second University of Naples, via Roma 29, 81031, Aversa, Italy
[c] Mork Family Department of Chemical Engineering and Material Science, Viterbi School of Engineering, University of Southern California, Los Angeles, CA, 90089, USA
[d] Department of Physics and Astronomy, Dornsife College of Letters, Arts, and Sciences, University of Southern California, Los Angeles, CA, 90089, USA
[e] Ming Hsieh Department of Electrical Engineering, Viterbi School of Engineering, University of Southern California, Los Angeles, CA, 90089, USA

ARTICLE INFO

Article history:
Received 10 August 2012
Received in revised form 20 February 2013
Accepted 1 March 2013
Available online 15 March 2013

Keywords:
Osmotic imbalance
Ion gradient
Permeabilization kinetics
Electroporation

ABSTRACT

Pulsed electric fields are used to permeabilize cell membranes in biotechnology and the clinic. Although molecular and continuum models provide compelling representations of the mechanisms underlying this phenomenon, a clear structural link between the biomolecular transformations displayed in molecular dynamics (MD) simulations and the micro- and macroscale cellular responses observed in the laboratory has not been established. In this paper, plasma membrane electropermeabilization is characterized by exposing Jurkat T lymphoblasts to pulsed electric fields less than 10 ns long (including single pulse exposures), and by monitoring the resulting osmotically driven cell swelling as a function of pulse number and pulse repetition rate. In this way, we reduce the complexity of the experimental system and lay a foundation for gauging the correspondence between measured and simulated values for water and ion transport through electropermeabilized membranes. We find that a single 10 MV/m pulse of 5 ns duration produces measurable swelling of Jurkat T lymphoblasts in growth medium, and we estimate from the swelling kinetics the ion and water flux that follows the electropermeabilization of the membrane. From these observations we set boundaries on the net conductance of the permeabilized membrane, and we show how this is consistent with model predictions for the conductance and areal density of nanoelectropulse-induced lipid nanopores.

1. Introduction

By altering the barrier function of the cell membrane in a non-lethal manner, electropermeabilization (electroporation) facilitates the entry of nucleic acids and pharmaceutical agents into living cells [1,2]. Clinical applications of electroporation include electrochemotherapy (enhancement of anti-tumor drug activity) [3], electrogene therapy (promotion of the uptake of cancer-suppressing genetic material) [4], and non-thermal ablation of cancer tissue [5–7]. Efficient optimization of the protocols used in these applications requires an expansion of our knowledge of the mechanisms of the restructuring of cell membranes that occurs in the presence of an applied electric field.

Investigations following the first reports of modifications of membrane conductance by electric fields [8–10] led to an empirical understanding of the electropermeabilization process [11–13] that was complemented by electrophysical models [14–20], and more recently corroborated by molecular dynamics (MD) simulations [21–26]. Taken together, these studies have given us a hypothetical physical mechanism for the poration of phospholipid bilayers, which can be expected to apply, at least in part, to the electropermeabilization of living cell membranes. It must be kept in mind, however, that the MD systems studied to date are highly simplified in comparison with a cell membrane, with one or two or at most three lipid and one or two cation species in bilayers with areas less than 200 nm^2, containing no membrane proteins or other intra- and extracellular associations.

As the availability of increasing computing power enables us to simulate more and more complex systems (larger and more heterogeneous bilayers with embedded proteins and intra- and extracellular attachments), we seek also a simplification of our experimental systems, to approach in our observations the primary events of the electropermeabilization process, separating them as much as possible from the myriad downstream consequences of breaching the cell membrane barrier with a large external electric field. At the intersecting trajectories of more and more accurate models and more and more fundamental experiments, we expect to find not only a better understanding of the physics of single, isolated lipid nanopores but also a mechanistic framework for manipulating populations of electric field-generated pores in the cells and tissues of living systems [27].

In this paper we simplify the experimental system in two ways. First, we minimize the duration of the permeabilizing event to less than 10 ns [28–31], and we include in our analysis cell responses to single pulses. In this way we reduce the number and the magnitude of secondary

* Corresponding author at: CNR-Institute for Electromagnetic Sensing of Environment (IREA), via Diocleziano 328, 80124, Naples, Italy. Tel.: +39 081 76 206 60; fax: +39 081 5705734.
E-mail address: romeo.s@irea.cnr.it (S. Romeo).

0005-2736/$ – see front matter © 2013 Elsevier B.V. All rights reserved.
http://dx.doi.org/10.1016/j.bbamem.2013.03.007

disturbances. The rationale for this approach can be explained by considering that when applying a train of pulses, each new pulse acts on cells that have been already affected by the preceding exposure, triggering a series of cascading events that increase the complexity of the phenomena to be analyzed. Applying only a single pulse simplifies the experimental conditions and the cellular responses. Similarly for pulse duration, as the field is applied for a longer and longer time, it is reasonable to expect that the initial primary effects of field-biomolecular structure interaction will be compounded. Therefore, short pulse studies like this one can help to unravel the complexity and to approach the most basic events of the electropermeabilization process.

Second, rather than use impermeant dyes as indicators of electroporation, we track the changes in cell volume that occur as a result of membrane permeabilization-induced osmotic imbalance [32–36]. Electropermeabilized membranes are conductive for Na^+, K^+, and Cl^-, so a permeabilized cell cannot maintain the normal transmembrane concentration gradients for these ions, a key component of the net cellular osmotic balance. In physiological media, because larger intracellular solutes cannot cross the permeabilized membrane, the intracellular osmolality becomes greater than the extracellular osmolality. This is countered by water influx into the cell, resulting in an increase in cell volume (cell swelling) [37,38]. The advantage of this approach compared to methods based on fluorescent, impermeant dyes for the study of electropermeabilization induced by nanosecond pulses is that the sensitivity of the latter is limited by the number and size of the pores created. Below a certain dose, the fluorescence emission from the small amount of dye that enters the cell is difficult to distinguish from background with affordable and flexible imaging and other detection systems. It has been demonstrated for nanosecond pulses that the process of pore creation dominates that of pore expansion, so the transport of even relatively small dye molecules through the nanometer-sized pores produced by nanosecond pulse exposure is much less than the flux of smaller species like calcium and monovalent ions [39]. Thus the analysis of cell swelling, which is not dependent on the dye selection and on the sensitivity of fluorescence detection methods, can be used for the study of plasma membrane electropermeabilization even in response to mild stresses (single, nanosecond-duration pulses), and for following the time dynamics of the phenomenon [38].

By exposing Jurkat T lymphoblasts to 5 ns, 10 MV/m pulsed electric fields, we are able to systematically analyze, using standard white light microscopic imaging, the resulting osmotically driven cell swelling as a function of pulse number (from 1 to 50) and pulse repetition rate (1 kHz or 1 Hz). From the rate and magnitude of the response, we characterize the dynamics of electropermeabilization under relatively unexplored pulsing conditions, and we extract values for ion and water flux through the permeabilized membrane.

This approach provides a simple and direct connection between simulations and experimental systems. By correlating observed swelling kinetics with rates of pore formation and ion and water transport obtained from molecular simulations and continuum representations, we establish reference points for improving the accuracy and applicability of the models, we elevate confidence in the validity of the mechanism for electropermeabilization that is emerging from MD studies, and we strengthen the physics-grounded foundation needed for methodological improvements in electroporation technology.

2. Materials and methods

2.1. Cell experiments

2.1.1. Cell culture

Jurkat T lymphoblasts (ATCC TIB-152, Manassas, VA) were grown in RPMI 1640 (Mediatech, Manassas, VA) containing 10% heat-inactivated fetal bovine serum (Gibco, Carlsbad, CA), 2 mM L-glutamine (Gibco), 50 U/mL penicillin (Gibco), and 50 μg/mL streptomycin (Gibco). Cells were maintained in exponential growth at 37 °C in a humidified, 5% CO_2 atmosphere.

2.1.2. Cell preparation

For pulse treatment, cells were concentrated to 2×10^7 cells/mL and in some cases incubated for 15 min with 0.5 μM calcein-AM (acetoxymethyl ester, Molecular Probes, Eugene, OR), which enhances visualization of the cell outline using fluorescence microscopy. After loading of the dye, cells were centrifuged and resuspended in fresh RPMI 1640 (or in some cases 150 mM NaCl) at 2×10^7 cells/mL. For exposure in presence of lanthanide or mercuric ions, $GdCl_3$ or $LaCl_3$ (Aldrich Chem. Co, Milwaukee, WI), 100 μM or 1 mM, or $HgCl_2$, 50 μM, was added to the cell suspension 5 min before pulse treatment.

2.1.3. Pulsed electric field exposures

For microscopic observation, cells were placed in a microchamber 100 μm wide, 30 μm deep, and 15 mm long, with platinum electrode walls on a glass microscope slide. A resonant-charged, solid-state Marx bank-driven, hybrid-core compression, diode-opening switch pulse generator designed and assembled at the University of Southern California [40] delivered 5 ns, 10 MV/m electrical pulses at a 1 kHz repetition rate (1 Hz where noted) to the microchamber electrodes mounted on the microscope stage in ambient atmosphere at room temperature.

2.1.4. DIC and fluorescence microscopy

Observations of live cells during and after pulse exposure were made with a Zeiss (Göttingen, Germany) Axiovert 200 epifluorescence microscope with 63× water immersion objective and Hamamatsu (Higashi-ku, Hamamatsu City, Japan) ImageEM EM-CCD camera. Captured images were analyzed with Hamamatsu SimplePCI and ImageJ (http://imagej.nih.gov/ij/) software. The cell perimeter was tracked using a freehand selection function, and then the area defined by the drawn perimeter was measured. To reduce variability, cells in the center of the exposure chamber, not adjacent to the electrode surfaces, were selected in the images captured immediately before pulsing, and then the same cells were analyzed in the post-pulse images. For each pulsing condition, at least 3 experiments were carried out, and a total of at least 30 cells were analyzed.

2.2. Molecular dynamics simulations

2.2.1. Simulation conditions and parameters

Simulations were performed using the GROMACS set of programs version 4.0.5 [41] on the University of Southern California High Performance Computing and Communications Linux cluster (http://www.usc.edu/hpcc/). Lipid topologies derived from OPLS united-atom parameters [42] were obtained from Peter Tieleman (http://moose.bio.ucalgary.ca). The Simple Point Charge (SPC) water model [43] was used, and all simulations were coupled to a temperature bath at 310 K with a relaxation time of 0.1 ps and a pressure bath at 1 bar with a relaxation time of 1 ps, each using a weak coupling algorithm [44]. Pressure was coupled semi-isotropically (using a compressibility of 4.5×10^{-5} bar^{-1}) normal to and in the plane of the membrane (NpT). Bond lengths were constrained using the LINCS algorithm [45] for lipids and SETTLE [46] for water. Short-range electrostatic and Lennard–Jones interactions were cut off at 1.0 nm. Long-range electrostatics was calculated with the PME algorithm [47] using fast Fourier transforms and conductive boundary conditions. Reciprocal-space interactions were evaluated on a 0.12 nm grid with fourth order B-spline interpolation. The parameter ewald_rtol, which controls the relative error for the Ewald sum in the direct and reciprocal space, was set to 10^{-5}. Periodic boundary conditions were employed to mitigate system size effects. Diffusion of water was calculated from mean square displacements over 50 ps using the 'g_msd' tool in GROMACS.

2.2.2. Systems and structures

All phospholipid systems contain 128 1-palmitoyl-2-oleoyl-*sn*-glycero-3-phosphatidylcholine (POPC) lipids and 8960 water molecules (70 waters/lipid), which results in a system box size of approximately 7 nm × 7 nm × 10 nm. To ensure that replicated simulations are independent, each atom is assigned a randomized velocity from a Maxwell distribution at the beginning of a simulation (a built-in function of GROMACS). POPC systems are equilibrated before electroporation by waiting until they reach a constant area per lipid — 0.66 nm^2.

2.2.3. Images

Molecular graphic images were generated with Visual Molecular Dynamics (VMD) [48].

3. Results and discussion

3.1. Electric pulse-induced cell swelling

Jurkat T lymphoblasts exposed to 5 ns, 10 MV/m electric pulses in physiological medium (RPMI 1640) exhibit an increase in cross-sectional area (Fig. 1) by as much as a factor of 1.5 (1.8-fold volume increase, if the cells were perfectly spherical) within 3 min after the pulses are delivered (Fig. 2). The rate of swelling is greatest immediately following pulse exposure, declining exponentially over tens of seconds, but not falling to zero after 3 min (Fig. 2). Cells were not observed to recover their initial volume, under the conditions in these experiments, even after 7 min, the longest monitoring time permitted by our apparatus. Cells do not respond uniformly, as shown in Fig. 1. The responses of individual cells vary not only in the magnitude of the volume increase, but also in the visual appearance of the cells during the first minute after pulsing. Some cells expand more or less uniformly, maintaining their roughly spherical shape. Others initially form one or more blebs of various sizes, which are subsumed as the cell continues to swell and recover its spheroidal geometry. An increase in cell area can be detected even after a single 5 ns, 10 MV/m pulse (Fig. 3).

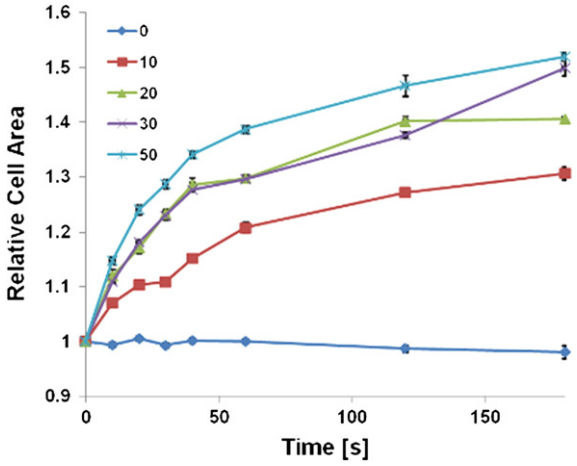

Fig. 2. Dose-dependent area increase of Jurkat cells after exposure to 0, 10, 20, 30 and 50 5 ns, 10 MV/m electric pulses delivered at 1 kHz. Note initial rapid swelling, which declines over about 1 min to a slower, but non-zero rate. Results are presented as mean ± standard error for at least 30 cells, from at least 3 independent experiments, for each pulsing condition.

Although this is the first systematic study of cell swelling following exposure to pulsed electric fields shorter than 10 ns, the phenomenon seems qualitatively similar to that reported for much longer pulses, so it is likely that the primary mechanisms are the same for short and long pulses [36,37]. The phenomenon of pulse-induced osmotic imbalance and the resulting cell swelling are consistent with the mechanistic hypothesis that nanosecond pulses open a large number of small pores on the plasma membrane, with a pore creation rate larger than the pore expansion one. Inorganic ions and small molecules, but not larger solutes, pass through these defects [20].

From the presented results, and building on conclusions supported by previous studies [32–36], we propose the following hypothetical

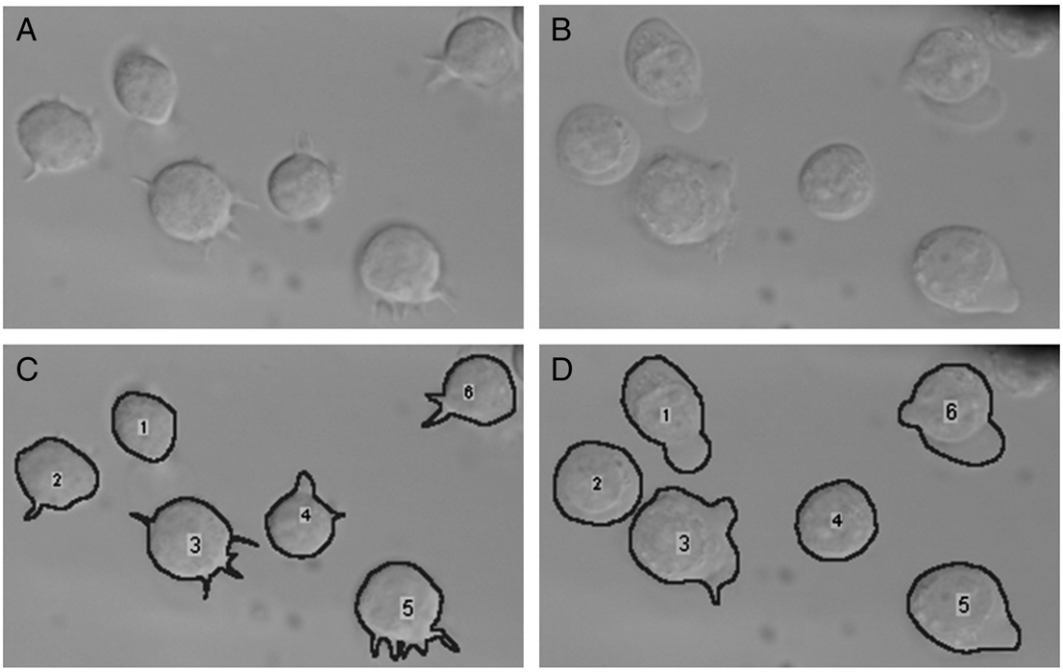

Fig. 1. Osmotic swelling after nanoelectropulse exposure. (A) Jurkat cells before pulse exposure. (B) Same cells 60 s after exposure to 30, 5 ns, 10 MV/m pulses at 1 kHz. (C), (D). Cells in (A) and (B) are outlined for area extraction with ImageJ. Note pulse-induced swelling, blebbing, and intracellular granulation and vesicle expansion, a result of the osmotic imbalance caused by electropermeabilization of the cell membrane.

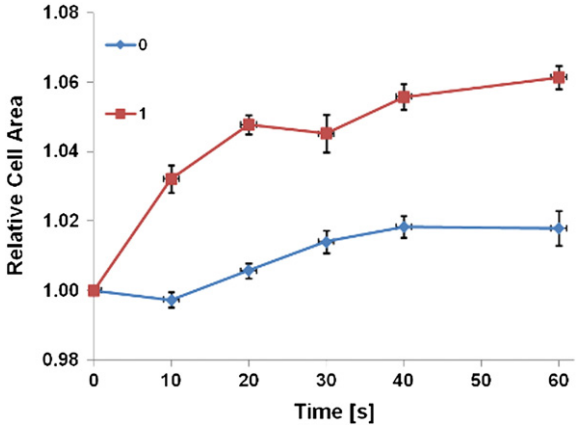

Fig. 3. Cell swelling can be reliably detected after even a single 5 ns, 10 MV/m pulse. Results are presented as mean ± standard error for at least 30 cells, from at least 3 independent experiments, for each pulsing condition.

sequence of events in Jurkat cells responding to 5 ns, 10 MV/m electric pulses delivered at 1 kHz. All of the observations we describe below are consistent with this scheme.

1. Pulse exposure results in the immediate formation of a dose-dependent number of lipid nanopores of a dose-dependent total area, large enough to allow passage of small inorganic ions [36]. These pores are formed during the 5 ns duration of a pulse.
2. Equilibration of intracellular and extracellular [Na^+], [K^+], and [Cl^-] by diffusive ion transport through the permeabilized membrane (presumably through the lipid nanopores but perhaps also through other structures) proceeds for several minutes [33,49,50].
3. During [Na^+], [K^+], and [Cl^-] equilibration, water flux (bidirectional under balanced conditions) becomes net positive inward, driven by the osmotic gradient caused by the reduction of the mobile ion concentration gradients and the remaining intracellular colloidal anions and other large molecules. This osmotically driven water influx is the primary cause of pulse-induced cell swelling [38].
4. When the [Na^+], [K^+], and [Cl^-] concentration gradients across the membrane reach zero (or some minimum value), water influx continues at a continually decreasing rate, as the internal osmolytes are diluted, until the ion-permeant structures (pores) close, allowing re-establishment of small ion concentration gradients, or until mechanical constraints become significant, or until the cell bursts.

3.2. Swelling is a function of the electrical impact dose

The mean swelling response of a population of cells as a function of the electrical impact dose, defined by Schoenbach et al. [51], is reported in Fig. 4a. At least for the first 60 s, the relative cell area scales with the square of the pulse count, probably a reflection of the stochastic character of electropore formation [14,52]. However, we find that our data can be better fit (Fig. 4b) by an equation of the type:

$$A_R(t) = E\tau N^x + k. \quad (1)$$

Here $A_R(t)$ is the pulse-number-dependent cross-sectional area of the cells, evaluated at each sampled time point up to 180 s post pulse, E and τ are the electric field amplitude in V/m and the pulse duration

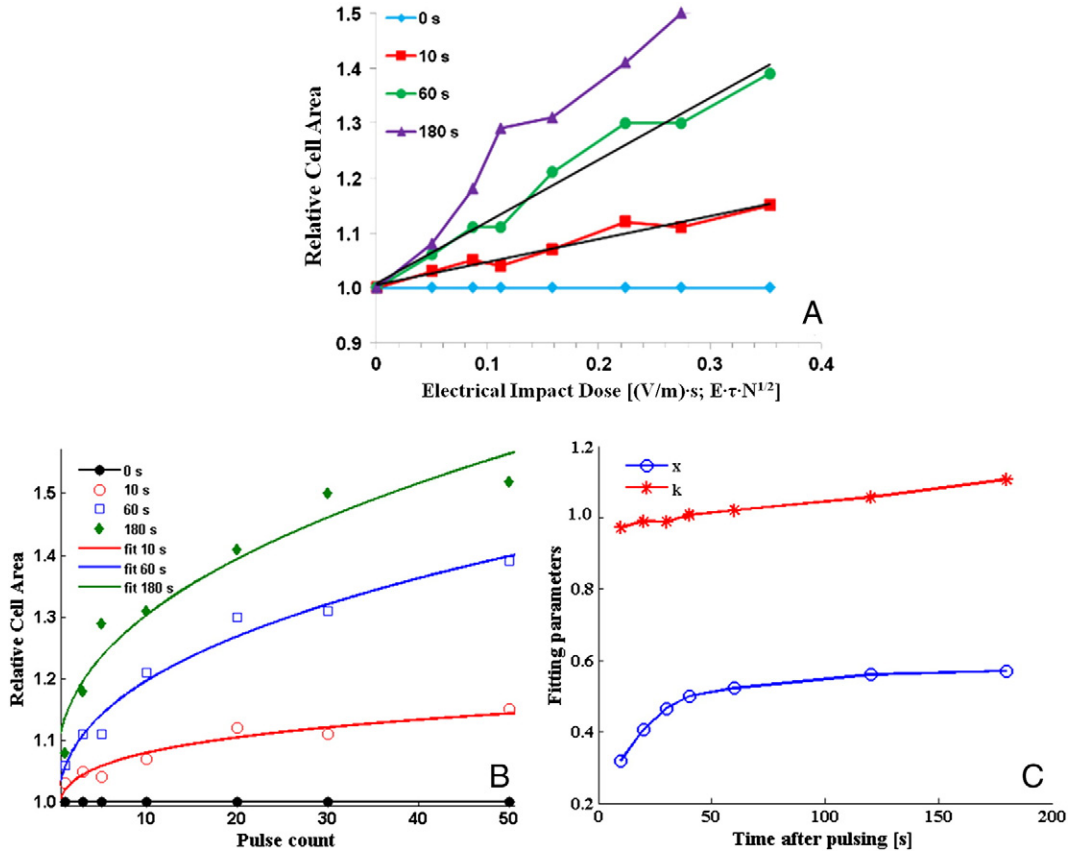

Fig. 4. Electric pulse-induced area increase dose-dependency. (A) The phenomenon is described for times up to about 60 s after exposure by the electrical impact dose factor, the product of the electric field, the pulse duration, and the square root of the number of pulses. The impact dose variable for these experiments is the pulse number N, which has the following values: 0, 1, 3, 5, 10, 20, 30, and 50. All pulses were 5 ns, 10 MV/m, delivered at 1 kHz. Straight gray lines are a linear fit to the swelling data at 10 s and 60 s; (B) fitting of the cell swelling data with Eq. (1); (C) fitting parameters over time.

in s, N is the pulse number (1, 3, 5, 10, 20, 30, and 50), and *x* and *k* are fitting parameters.

In Fig. 4b, the new data fitting is reported at 0, 10, 60 and 180 s after pulsing, while the behavior of the fitting parameters over the considered time interval is shown in Fig. 4c. The tendency clearly deviates from the model defined in [51] since the parameter *x*, which gives the scaling law with respect to pulse number, is not exactly 0.5, but slowly increases from less than 0.5 and approaches 0.6 at the end of the observation time. On the other hand, *k* can be interpreted as the relative cell area when the pulse number is N = 0, and the fact that it is not exactly 1 may reflect the uncertainty of our estimation of the cell area.

The model defined by Schoenbach and co-workers for the dependence of bioelectric effects on pulse parameters is based on the hypothesis of a "random rotation" of the cell, with respect to the direction of the applied electric field, between consecutive pulses. This assumption holds true if the recovery time of the cell membrane is long compared to the time between pulses, and if the cell rotation is random. Accordingly, it is expected that for high repetition rate pulsing the cell rotation between pulses will be negligible, and the observed effects will scale with N^x, where x is a value larger than 0.5 and eventually approaching 1. In our pulsing conditions, with a 1 kHz repetition rate, the hypothesis for the random rotation underlying the model is likely not respected, but the observed response is definitely non-linear with respect to pulse number.

A possible interpretation of this intermediate situation might be that if the first pulses induce a permeabilization of certain sites of the plasma membrane, consecutive pulses acting on the same sites – because the cell is not rotating – will not add linearly to the cumulative effect. The more pulses are delivered, the more sites that are permeabilized, and the less likely it is that a subsequent pulse will make a new pore. This could easily produce a fractional exponent in the neighborhood of 0.5. Higher or lower repetition rates could combine with this mechanism to produce a large number of functional relations.

3.3. Electric pulse-induced water flux

Fig. 3 shows a relative cell area increase of 3% over the 10 s immediately following a single 5 ns, 10 MV/m pulse. For a cell radius of 5 μm, that is a volume change of 2.3×10^{-17} m^3, which corresponds to 7.7×10^{11} water molecules over 10 s. If the expansion were linear, this would be a net 77 water molecules entering the cell per nanosecond. If the swelling is described by a decaying exponential, then the initial rate is higher. For an initial approximation we assume 77 H_2O/ns. Even though this is a rough number, it provides a basis for comparison with experimentally known transport rates of water. After some additional calculations, discussed below, some approximate ion transport rates can be derived as well, which can be used to set boundaries for pore density and area.

It might be expected that water passes through the lipid nanopores created by the pulse, and some net water transport undoubtedly does occur this way, and perhaps through aquaporin channels as well. But the water permeability of lipid bilayers and cell membranes ($P_f = 1.3 \times 10^{-4}$ $m \cdot s^{-1}$ for POPC [53]; $P_f = 6.7 \times 10^{-6}$ $m \cdot s^{-1}$ for a more complex bilayer [54]), is high enough to account for a significant amount of the observed pulse-induced water influx. Lipid nanopores are required for the ion transport and concentration equilibration that occurs after pulse exposure, and which drives the osmotic flow of water into the cell, but non-permeabilized membrane leakage pathways are largely sufficient for the post-pulse water entry itself.

3.4. MD simulation of water permeation of an intact lipid bilayer

Molecular simulations reveal how water permeates a lipid bilayer without pore formation [55,56]. About once per nanosecond in simulations of 50 nm^2 POPC bilayers at 310 K [57], an isolated water molecule crosses from one leaflet of an intact bilayer to the other (Fig. 5). No pore is involved, and application of a porating electric field has little effect on either the frequency or the direction of these random, diffusive crossing events. In simple bilayer systems the primary determinant of the rate of crossing from one side of the membrane to the other (expressed experimentally as the permeability coefficient) is the area per lipid [53]. Systems with a smaller area per lipid have smaller permeability coefficients [58]. Although detailed calculations would be premature at the present level of accuracy and understanding of the correspondence between MD simulations of lipid bilayers and living cell membranes, we can translate the random and bidirectional 1 H_2O per nanosecond per 50 nm^2 that we observe in our POPC simulations to an osmotically driven (initially 100 mOsm) net transport of about 10^4 H_2O per nanosecond per cell, declining exponentially as the ion concentration imbalance is reduced.

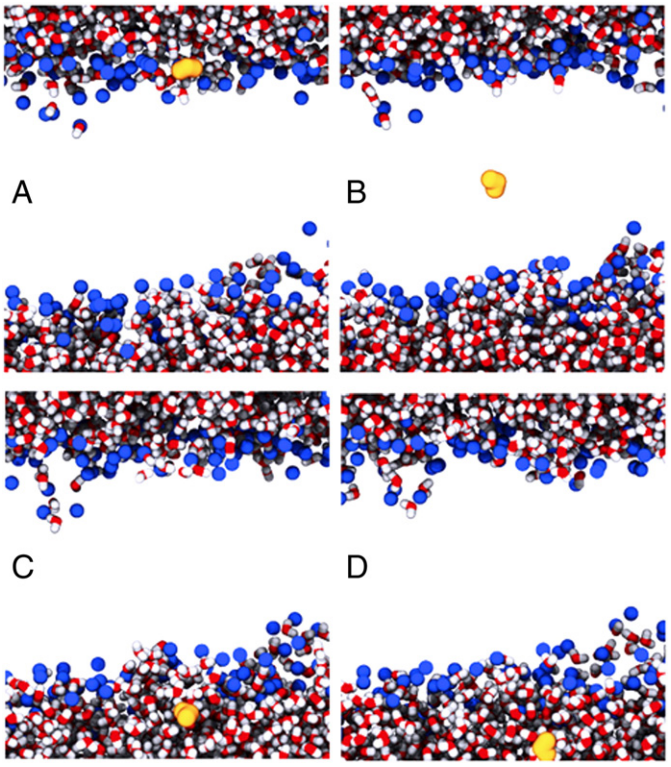

Fig. 5. Random permeation of an intact POPC bilayer. A single H_2O molecule crosses the phospholipid bilayer interface. Applied electric field is 340 MV/m downward in the diagram. (A) 0 ps, (B) 100 ps, (C) 200 ps, (D) 300 ps. Only acyl oxygens and water molecules in the interface are shown. The crossing water molecule is enlarged and colored yellow. Light blue spheres are acyl oxygens; red and white atoms are water; the empty space in the middle of figures between two water phases represents the hydrocarbon region of the lipid bilayer. From a system containing 128 POPC, 4480 H_2O, at 310 K, 1 bar.

3.5. Electric pulse-induced ion flux

Ion permeabilities for intact membranes are several orders of magnitude lower than water permeability. This membrane barrier function permits the establishment of the Na^+ and K^+ concentration gradients that result primarily from the operation of Na^+/K^+-ATPase pumps and K^+ leak channels, and which are an essential component in the maintenance of physiological osmotic balance. Electropermeabilization of the membrane bypasses this active regulation by providing pathways for Na^+ and K^+ transport that are not under the control of the cell. We hypothesize that the lipid nanopores seen in MD simulations, and for which there is some experimental evidence [28,29,37], are the structures through which this ion flux occurs. The formation of these

nanopores during electric pulse exposures leads to an osmotic imbalance which the cell cannot quickly restore, and the result is colloidal osmotic swelling [38].

Although it is not possible from our data to rule out the possible participation of membrane protein channels in this process, we have two sets of observations that are consistent with a major role for lipid nanopores and a minor role for other potential mechanisms.

First, we see no significant inhibition of nanoelectropulse-induced swelling by the ion channel blockers Gd^{3+} and La^{3+} [59–62] at concentrations of 0.1 mM and 1 mM (Table 1). This is only a non-specific and imprecise indication, of course, but this result stands in interesting contrast to a report of Gd^{+3} inhibition of osmotic swelling [37]. Pulse characteristics and exposure conditions, however, are quite different in the two cases. Our pulses are 5 ns, 10 MV/m; the pulses in [37] are 60 ns and 600 ns, 1.2 MV/m. Longer pulses may induce a more extensive membrane restructuring that is Gd^{3+}-sensitive.

It is important to note, however, that lanthanide ions promote the precipitation of lanthanide phosphates in cell culture media depending on time and concentration. The experiments using lanthanides in complete culture medium were carefully carried out to take this into account, and no precipitation was observed throughout the exposure and image capturing time. Of course this does not rule out the formation of soluble complexes, but we think it is important to observe cells under optimum, minimally disturbed growth conditions. Experiments in NaCl were performed as a check on the possibility of lanthanide chelation and complex formation by phosphates and other constituents of the complex growth medium, with negative results. Although it cannot be excluded that the lack of effect of lanthanides might be due to complex formation in culture medium, this possibility does not affect the validity of our trials, as a simple check to see if these ions have an effect under the conditions of our experiments.

Second, to see whether the opening of aquaporin channels may be involved in the swelling response, including even possibly voltage-sensitive aquaporin channels [63], we carried out pulse exposures in the presence of mercuric ion, an inhibitor of aquaporins [64,65]. The results were similar to those obtained with the lanthanide ions. In these experiments Hg^{2+} had no significant effect on nanoelectropulse-induced osmotic swelling of Jurkat cells (Table 1).

3.6. The rate and extent of nanoelectropulse-induced cell swelling is dependent on the pulse repetition rate

Previously we have reported that the extent of the nanoelectropulse-induced influx of the normally impermeant fluorescent dye YO-PRO-1 into Jurkat cells is dependent on the pulse repetition rate [29]. For a given number of pulses, the amount of YO-PRO-1 that enters the cell is considerably greater for a pulse repetition rate of 1 kHz than it is for lower pulse repetition rates. Also Sun et al. have found that B16 murine melanoma cells pulsed at 100 Hz (10 ns, 15 MV/m) consistently take up more trypan blue than cells pulsed at 1 or 10 Hz [66]. We find a similar dependency when cell swelling is taken as an indicator of permeabilization (Fig. 6). This is again in contrast to results reported for longer but still sub-microsecond pulses [67]. These differences in repetition-rate dependencies for the magnitude and the Gd^{3+}-sensitivity (noted above) of the swelling response suggest that longer pulses (≥60 ns) produce a qualitatively different restructuring of the membrane than is produced by 5 ns pulses.

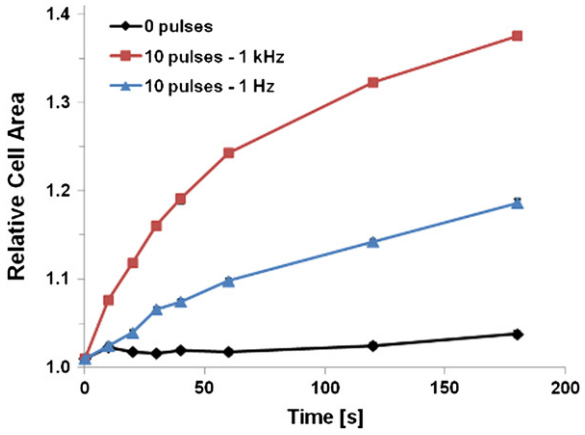

Fig. 6. Rate and extent of pulse-induced swelling is greater at higher pulse repetition rates. Results are presented as mean ± standard error for at least 30 cells, from at least 3 independent experiments for each pulsing condition.

Considering now only the 5 ns pulses used in the work reported here, we can hypothesize that high-repetition-rate (1 kHz) pulses either expand the area of the pores formed by the first pulse or they create new pores or both. If high-repetition-rate pulses only expand the pores formed by the first pulse, then the expansion must produce more pore area per pulse than multiple pulses widely separated in time. To distinguish among these possibilities we will need to learn more about the pore density and the population distribution of the pore area.

An alternate explanation assumes that some pore repair processes initiated by membrane permeabilization take longer than a time on the order of 1 ms. When a second pulse is delivered in 1 ms or less after the first pulse, the permeabilizing damage has not yet been repaired, or has been only partially repaired, and so the damage is compounded. The result is a greater effect at a higher repetition rate. At lower repetition rates, when more than 1 ms passes between pulses, there is sufficient time for this repair process to complete, and the damage is merely additive. Only further observations and more accurate modeling can resolve these possibilities, but the use of osmotic swelling as an indicator of membrane permeabilization, with its sensitivity to solute molecular size [38], lends itself to the kind of focused study that is required.

3.7. Nanoelectropulse-induced cell swelling is caused by diffusive loss of intracellular-extracellular ion concentration gradients and osmotically driven water influx

We have extracted from the swelling data a simple functional expression that describes our observational data and which

Table 1
Pulse-induced Jurkat cell swelling in presence of lanthanides or mercury ions.

	0 s				10 s				60 s			
	RPMI alone	Gd^{3+} 100 μM	La^{3+} 100 μM	Hg^{2+} 50 μM	RPMI alone	Gd^{3+} 100 μM	La^{3+} 100 μM	Hg^{2+} 50 μM	RPMI alone	Gd^{3+} 100 μM	La^{3+} 100 μM	Hg^{2+} 50 μM
0 p	1.0	1.0	1.0	1.0	0.99 ± 0.0040	1.0 ± 0.0050	1.0 ± 0.013	0.99 ± 0.0080	1.0 ± 0.0040	0.99 ± 0.0070	0.99 ± 0.013	1.0 ± 0.012
10 p	1.0	1.0	1.0	1.0	1.1 ± 0.0020	1.0 ± 0.0060	1.0 ± 0.0060	1.03 ± 0.012	1.2 ± 0.0090	1.1 ± 0.0020	1.1 ± 0.013	1.2 ± 0.015
50 p	1.0	1.0	1.0	1.0	1.2 ± 0.0060	1.2 ± 0.0030	1.08 ± 0.0090	1.1 ± 0.011	1.4 ± 0.0070	1.3 ± 0.0070	1.3 ± 0.020	1.4 ± 0.017

Relative cell area increase over time in Jurkat cells exposed to 0, 10, or 50 pulses in RPMI alone or in presence of $GdCl_3$ or $LaCl_3$ (100 μM) or $HgCl_2$ (50 μM). Similar results were obtained when cells were suspended in 150 mM NaCl as pulsing buffer. Data are presented as mean ± standard error over three independent experiments (at least 30 cells for each condition).

corresponds to the simple mechanism for the phenomenon outlined above,

$$A_R(t) = b \cdot exp(-ct) + at + d \quad (2)$$

where $A_R(t)$ is the time-dependent relative cross-sectional area of the cell, a is the slope of the linear relative area increase, b is the initial point of exponential relative area increase (at $t = 0$), d is the initial point of linear relative area increase, and c is the exponential scaling factor. Note that at $t = 0$, $b + d = 1$ (the area does not begin to increase until just after the pulse exposure). Fig. 7 shows how this function can be fit to the swelling response over a wide range of exposures — 1, 10, and 50 pulses.

The nanoelectropulse-induced swelling response can now be analyzed as an overlapping sequence of phenomena associated with membrane permeabilization, diffusive ion transport, and the osmotic flow of water. We see now in this functional form the same four steps we proposed at the beginning of this discussion: 1. lipid nanopore formation (and perhaps other electropermeabilization-associated restructuring of the cell membrane); 2. equilibration of intracellular and extracellular concentrations of sodium, potassium, and chloride ions ($[Na^+]_i$, $[K^+]_i$, and $[Cl^-]_i$] and $[Na^+]_e$, $[K^+]_e$, and $[Cl^-]_e$), at an exponentially decreasing rate corresponding to the term be^{-ct}; 3. net inward H_2O flux, increasing during the period of small ion equilibration, which creates the osmotic imbalance, that drives the water flow; and 4. continuing inward H_2O flux, at a continually decreasing rate as the internal osmolytes are diluted.

The coefficient c has units of inverse time, so we may consider $1/c$ to represent a time constant for the overall equilibration of small ions (primarily Na^+ and K^+) through the permeabilized membrane.

Although we understand that we risk oversimplifying a complex situation, it may be instructive as a guide to further experimentation and better models to consider the implications of the value of this constant that we extract from our data. For the simplest case — single-pulse-induced swelling — we obtain values for τ ($1/c$) of about 10 s [68]. Continuing our simple interpretation, we can then say that the ion concentration gradients are reduced by 1/e in the period of one time constant.

Consider these (also approximate) numbers for K^+ concentration: 105 mM for $[K^+]_i$ and intracellular and 5 mM $[K^+]_e$, before permeabilization. We choose K^+ because it is expected to be more rapidly transported through lipid nanopores than Na^+ [69], but any of the three major ions could have been chosen as an example, since our model includes also Na^+ influx and Cl^- transport as well. We should expect that the initial gradient of about 100 mM (105 mM − 5 mM), will be reduced by a factor e to about 37 mM during one time constant.

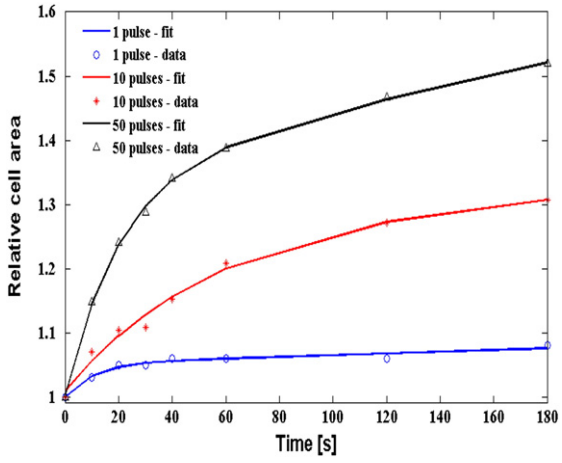

Fig. 7. A simple exponential function describes the time course of nanoelectropulse-induced cell swelling. The comparison between experimental data and the fitting function is reported for cell swelling after 1, 10 and 50 pulses.

Since $[K^+]_e$ will remain essentially unchanged for normal cell suspensions (where the volume fraction of cells is less than 10%), this means that $[K^+]_i$ will change by about 37 mM in 10 s. For a typical Jurkat cell with a radius of 5 μm, that corresponds to about 1.2×10^{10} K^+ transported out of each cell in 10 s, and 1.2 K^+ in 1 ns. These numbers, although neither general nor conclusive, are consistent with experimental observations reported for ion transport rates through artificial membranes and electropermeabilized cells [50,70].

MD systems for simulating ion transport through electropores in lipid bilayers [70] have not yet provided solid values for ion conductance, so the connection between the molecular-scale implications of cell swelling experiments discussed above and the behavior of lipid nanopores has not yet been charted.

4. Conclusions

We have demonstrated in this paper that osmotically driven cell swelling can be used as a sensitive method for studying plasma membrane electropermeabilization induced by very short and very intense pulsed electric fields.

We have presented evidence that a single 5 ns, 10 MV/m electric pulse permeabilizes living cell membranes. Moreover we have characterized the swelling response as a function of pulse number and repetition rate, demonstrating that it increases with the number of pulses delivered, is frequency-dependent (increasing when pulses are delivered at higher repetition rate), and that, in our experimental conditions, it is not sensitive to the presence of the lanthanide ions Gd^{3+} and La^{3+} (ion channel blockers), or mercuric ions, Hg^{2+}, (aquaporin channel inhibitor) in the external medium. Our results are consistent with the idea that the primary permeabilizing event leading to cell swelling is the formation of lipid pores in the plasma membrane.

The swelling kinetics can be described with a functional expression that matches a hypothetical mechanism for permeabilization-induced osmotic swelling — an initial loss of the normal physiological inorganic ion gradients followed by an influx of water in response to the colloidal ion imbalance that remains after permeabilization. In this model, membrane permeabilization is required for the initial ion flux but not for the subsequent water flux, which can occur through normal water leakage pathways.

Although further investigations and more refined models are needed to clarify the details of the mechanisms underlying electric pulse-induced membrane permeabilization, the approach adopted in this study allowed us to address the most basic events of the electroporation phenomenon and to establish a simple but explicit connection between MD simulations and experimental observations.

Acknowledgements

We thank Andrei G. Pakhomov, Olga N. Pakhomova, Justin Teissié, D. Peter Tieleman, James C. Weaver, and Olga Zeni for stimulating discussions, helpful suggestions, and probing comments. Computing resources were provided by the USC Center for High Performance Computing and Communications. This work was made possible in part by support from the Air Force Office of Scientific Research. SR was supported in part by the Second University of Naples.

References

[1] E. Neumann, M. Schaefer-Ridder, Y. Wang, P.H. Hofschneider, Gene transfer into mouse lyoma cells by electroporation in high electric fields, EMBO J. 1 (1982) 841–845.
[2] M.P. Rols, Electropermeabilization, a physical method for the delivery of therapeutic molecules into cells, Biochim. Biophys. Acta 1758 (2006) 423–428.
[3] M. Marty, G. Sersa, J.R. Garbay, J. Gehl, C.G. Collins, M. Snoj, V. Billard, P.F. Geertsen, J.O. Larkin, D. Miklavcic, I. Pavlovic, S.M. Paulin-Kosir, M. Cemazar, N. Morsli, Z. Rudolf, C. Robert, G.C. O'Sullivan, L.M. Mir, Electrochemotherapy — an easy, highly effective and safe treatment of cutaneous and subcutaneous metastases: results of ESOPE (European Standard Operating Procedures of Electrochemotherapy) study, Eur. J. Cancer Suppl. 4 (2006) 3–13.

[4] L.C. Heller, R. Heller, Electroporation gene therapy preclinical and clinical trials for melanoma, Curr. Gene. Ther. 10 (2010) 312–317.
[5] B. Rubinsky, Irreversible electroporation in medicine, Technol. Cancer Res. Treat. 6 (2007) 255–260.
[6] E.B. Garon, D. Sawcer, P.T. Vernier, T. Tang, Y. Sun, L. Marcu, M.A. Gundersen, H.P. Koeffler, In vitro and in vivo evaluation and a case report of intense nanosecond pulsed electric field as a local therapy for human malignancies, Int. J. Cancer 121 (2007) 675–682.
[7] R. Nuccitelli, X. Chen, A.G. Pakhomov, W.H. Baldwin, S. Sheikh, J.L. Pomicter, W. Ren, C. Osgood, R.J. Swanson, J.F. Kolb, S.J. Beebe, K.H. Schoenbach, A new pulsed electric field therapy for melanoma disrupts the tumor's blood supply and causes complete remission without recurrence, Int. J. Cancer 125 (2009) 438–445.
[8] R. Staempfli, M. Willi, Membrane potential of a Ranvier node measured after electrical destruction of its membrane, Experientia 13 (1957) 297–298.
[9] H.G.L. Coster, A quantitative analysis of the voltage–current relationships of fixed charge membranes and the associated property of "punch-through", Biophys. J. 5 (1965) 669–686.
[10] W.A. Hamilton, A.J.H. Sale, Effect of high electric fields on microorganisms. II. Mechanisms of action of the lethal effect, Biochim. Biophys. Acta 148 (1967) 789–800.
[11] U. Zimmermann, G. Pilwat, F. Riemann, Dielectric breakdown of cell membranes, Biophys. J. 14 (1974) 881–899.
[12] I.G. Abidor, V.B. Arakelian, L.V. Chernomordik, Yu.A. Chizmadzhev, V.F. Pastushenko, M.R. Tarasevich, Electric breakdown of bilayer lipid membranes. I. The main experimental facts and their qualitative discussion, Bioelectrochem. Bioenerg. 6 (1979) 37–52.
[13] Yu.A. Chizmadzhev, I.G. Abidor, Membranes in strong electric fields, Bioelectrochem. Bioenerg. 7 (1980) 83–100.
[14] I.P. Sugar, E. Neumann, Stochastic model for electric field-induced membrane pores, electroporation, Biophys. Chem. 19 (1984) 211–225.
[15] D. Popescu, C. Rucareanu, Gh. Victor, A model for the appearance of statistical pores in membranes due to self oscillations, Bioelectrochem. Bioenerg. 25 (1991) 91–103.
[16] J.C. Weaver, Yu.A. Chizmadzhev, Theory of electroporation: a review, Bioelctrochem. Bioenerg. 41 (1996) 135–160.
[17] K.A. DeBruin, W. Krassowska, Electroporation and shock-induced transmembrane potential in a cardiac fiber during defibrillation strength shocks, Ann. Biomed. Eng. 26 (1998) 584–596.
[18] J.C. Neu, W. Krassowska, Asymptotic model of electroporation, Phys. Rev. E 59 (1998) 3471–3482.
[19] J.C. Weaver, Electroporation of biological membranes from multicellular to nanoscale, IEEE Trans. Dielectr. Electr. Insul. 10 (2003) 754–768.
[20] Z. Vasilkoski, A.T. Esser, T.R. Gowrishankar, J.C. Weaver, Membrane electroporation: the absolute rate equation and nanosecond time scale pore creation, Phys. Rev. E 74 (2006) 021904.
[21] D.P. Tieleman, The molecular basis of electroporation, BMC Biochem. 5 (2004) 10.
[22] A.A. Gurtovenko, I. Vattulainen, Pore formation coupled to ion transport through lipid membranes as induced by transmembrane ionic charge imbalance: atomistic molecular dynamics study, J. Am. Chem. Soc. 127 (2005) 17570–17571.
[23] Q. Hu, R.P. Joshi, K.H. Schoenbach, Simulations of nanopore formation and phosphatidylserine externalization in lipid membranes subjected to a high-intensity, ultrashort electric pulse, Phys. Rev. E Stat. Nonlinear Soft Matter Phys. 72 (2005) 031902.
[24] M. Tarek, Membrane electroporation: a molecular dynamic simulation, Biophys. J. 88 (2005) 4045–4053.
[25] P.T. Vernier, M.J. Ziegler, Y. Sun, W.V. Chang, M.A. Gundersen, D.P. Tieleman, Nanopore formation and phosphatidylserine externalization in a phospholipid bilayer at high transmembrane potential, J. Am. Chem. Soc. 128 (2006) 6288–6289.
[26] M.L. Fernandez, G. Marshall, F. Sagues, R. Reigada, Structural and kinetic molecular dynamics study of electroporation in cholesterol-containing bilayers, J. Phys. Chem. B 114 (2010) 6855–6865.
[27] J. Teissie, M. Golzio, M.P. Rols, Mechanisms of cell membrane electropermeabilization: a mini review of our present (lack of?) knowledge, Biochim. Biophys. Acta 1724 (2005) 270–280.
[28] R. Benz, U. Zimmermann, Pulse-length dependence of the electrical breakdown in lipid bilayer membranes, Biochim. Biophys. Acta 597 (1980) 637–642.
[29] P.T. Vernier, Y. Sun, M.A. Gundersen, Nanoelectropulse-driven membrane perturbation and small molecule permeabilization, BMC Cell Biol. 7 (2006) 37.
[30] P.T. Vernier, Y. Sun, M.T. Chen, M.A. Gundersen, G.L. Craviso, Nanosecond electric pulse-induced calcium entry into chromaffin cells, Bioelectrochemistry 73 (2008) 1–4.
[31] S. Wang, J. Chen, M.T. Chen, P.T. Vernier, M.A. Gundersen, M. Valderrábano, Cardiac myocyte excitation by ultrashort high-field pulses, Biophys. J. 96 (2009) 1640–1648.
[32] J.F. Hoffman, Physiological characteristics of human red blood cell ghosts, J. Gen. Physiol. 42 (1958) 9–28.
[33] K. Kinosita Jr., T.T. Tsong, Hemolysis of human erythrocytes by transient electric field, Proc. Natl. Acad. Sci. U. S. A. 74 (1977) 1923–1927.
[34] M. Golzio, M.P. Mora, C. Raynaud, C. Delteil, J. Teissié, M.P. Rols, Control by osmotic pressure of voltage-induced permeabilization and gene transfer in mammalian cells, Biophys. J. 74 (1998) 3015–3022.
[35] M.M. Claessens, F.A. Leermakers, F.A. Hoekstra, M.A. Stuart, Osmotic shrinkage and reswelling of giant vesicles composed of dioleoylphosphatidylglycerol and cholesterol, Biochim. Biophys. Acta 1778 (2008) 890–895.
[36] A.G. Pakhomov, A.M. Bowman, B.L. Ibey, F.M. Andrè, O.N. Pakhomova, K.H. Schoenbach, Lipid nanopores can form a stable, ion channel-like conduction pathway in cell membrane, Biochem. Biophys. Res. Commun. 385 (2009) 181–186.
[37] F.M. André, M.A. Rassokhin, A.M. Bowman, A.G. Pakhomov, Gadolinium blocks membrane permeabilization induced by nanosecond electric pulses and reduces cell death, Bioelectrochemistry 79 (2010) 95–100.
[38] O.M. Nesin, O.N. Pakhomova, S. Xiao, A.G. Pakhomov, Manipulation of cell volume and membrane pore comparison following single cell permeabilization with 60- and 600-ns electric pulses, Biochim. Biophys. Acta 1808 (2011) 792–801.
[39] K.C. Smith, J.C. Weaver, Active mechanisms are needed to describe cell responses to submicrosecond megavolt-per-meter pulses: cell models for ultrashort pulses, Biophys. J. 95 (2008) 1547–1563.
[40] J.M. Sanders, A. Kuthi, Y.H. Wu, P.T. Vernier, M.A. Gundersen, A linear, single-stage, nanosecond pulse generator, for delivering intense electric fields to biological loads, IEEE Trans. Dielectr. Electr. Insul. 16 (2009) 1048–1054.
[41] B. Hess, C. Kutzner, D. Van der Spoel, E. Lindahl, GROMACS 4: algorithms for highly efficient, load-balanced, and scalable molecular simulation, J. Chem. Theory Comput. 4 (2008) 435–447.
[42] O. Berger, O. Edholm, F. Jänhig, Molecular dynamics simulations of a fluid bilayer of dipalmitoylphosphatidylcholine at full hydration, constant pressure, and constant temperature, Biophys. J. 72 (1997) 2002–2013.
[43] H.J.C. Berendsen, J.P.M. Postma, W.F. van Gunsteren, J. Hermans, Interaction models for water in relation to protein hydration, in: B. Pullman (Ed.), Intermolecular Forces, Reidel/Dordrecht, Netherlands, 1981, pp. 331–342.
[44] H.J.C. Berendsen, J.P.M. Postma, W.F. van Gunsteren, A. Dinola, J.R. Haak, Molecular dynamics with coupling to an external bath, J. Chem. Phys. 81 (1984) 3684–3690.
[45] B. Hess, H. Bekker, H.J.C. Berendsen, J.G.E.M. Fraaije, LINCS: a linear constraint solver for molecular simulations, J. Comput. Chem. 18 (1997) 1463–1472.
[46] S. Miyamoto, P.A. Kollman, SETTLE: an analytical version of the SHAKE and RATTLE algorithms for rigid water models, J. Comput. Chem. 13 (1992) 952–962.
[47] U. Essmann, L. Perera, M.L. Berkowitz, T. Darden, H. Lee, L.G. Pedersen, A smooth particle mesh Ewald method, J. Chem. Phys. 98 (1995) 10089–10092.
[48] W. Humphrey, A. Dalke, K. Schulten, VMD: visual molecular dynamics, J. Mol. Graph. 14 (1996) 33–38, (27–8).
[49] K. Schwister, B. Deuticke, Formation and properties of aqueous leaks induced in human erythrocytes by electrical breakdown, Biochim. Biophys. Acta 816 (1985) 332–348.
[50] G. Saulis, S. Satkauskas, R. Praneviciūte, Determination of cell electroporation from the release of intracellular potassium ions, Anal. Biochem. 360 (2007) 273–281.
[51] K.H. Schoenbach, R.P. Joshi, S.J. Beebe, C.E. Baum, A scaling law for membrane permeabilization with nanopulses, IEEE Trans. Dielectr. Electr. Insul. 16 (2009) 1224–1235.
[52] T.R. Gowrishankar, J.C. Weaver, Electrical behavior and pore accumulation in a multicellular model for conventional and supra-electroporation, Biochem. Biophys. Res. Commun. 349 (2006) 643–653.
[53] J.C. Mathai, S. Tristram-Nagle, J.F. Nagle, M.L. Zeidel, Structural determinants of water permeability through the lipid membrane, J. Gen. Physiol. 131 (2008) 69–76.
[54] A.V. Krylov, P. Pohl, M.L. Zeidel, W.G. Hill, Water permeability of asymmetric planar lipid bilayers: leaflets of different composition offer independent and additive resistances to permeation, J. Gen. Physiol. 118 (2001) 333–340.
[55] S.J. Marrink, H.J.C. Berendsen, Simulation of water transport through a lipid membrane, J. Phys. Chem. 98 (1994) 4155–4168.
[56] S.J. Marrink, H.J.C. Berendsen, Permeation process of small molecules across lipid membranes studied by molecular dynamics simulations, J. Phys. Chem. 100 (1996) 16729–16738.
[57] P.T. Vernier, Z.A. Levine, M.A. Gundersen, Water Bridges in Electropermeabilized Phospholipid Bilayers, Proc. IEEE 101 (2) (2013) 494–504.
[58] R. Vácha, M.L. Berkowitz, P. Jungwirth, Molecular model of a cell plasma membrane with an asymmetric multicomponent composition: water permeation and ion effects, Biophys. J. 96 (2009) 4493–4501.
[59] X.C. Yang, F. Sachs, Block of stretch-activated ion channels in *Xenopus* oocytes by gadolinium and calcium ions, Science 243 (1989) 1068–1071.
[60] S. Boitano, M.J. Sanderson, E.R. Dirksen, A role for Ca^{2+}-conducting ion channels in mechanically-induced signal transduction of airway epithelial cells, J. Cell Sci. 107 (1994) 3037–3044.
[61] C. Aussel, R. Marhaba, C. Pelassy, J.P. Breittmayer, Submicromolar La^{3+} concentrations block the calcium release-activated channel, and impair CD69 and CD25 expression in CD3- or thapsigargin-activated Jurkat cells, Biochem. J. 313 (1996) 909–913.
[62] J. Lee, A. Ishihara, G. Oxford, B. Johnson, K. Jacobson, Regulation of cell movement is mediated by stretch-activated calcium channels, Nature 400 (1999) 382–386.
[63] J.S. Hub, C. Aponte-Santamaria, H. Grubmuller, B.L. de Groot, Voltage-regulated water flux through aquaporin channels in silico, Biophys. J. 99 (2010) L97–L99.
[64] Y. Hirano, N. Okimoto, I. Kadohira, M. Suematsu, K. Yasuoka, M. Yasui, Molecular mechanisms of how mercury inhibits water permeation through aquaporin-1: understanding by molecular dynamics simulation, Biophys. J. 98 (2010) 1512–1519.
[65] G.M. Preston, J.S. Jung, W.B. Guggino, P. Agre, The mercury-sensitive residue at cysteine 189 in the CHIP28 water channel, J. Biol. Chem. 268 (1993) 17–20.
[66] Y. Sun, S. Xiao, J.A. White, J.F. Kolb, M. Stacey, K.H. Schoenbach, Compact, nanosecond, high repetition rate, pulse generator for bioelectric studies, IEEE Trans. Dielectr. Electr. Insul. 14 (2007) 863–870.
[67] O.N. Pakhomova, B.W. Gregory, V.A. Khorokhorina, A.M. Bowman, S. Xiao, A.G. Pakhomov, Electroporation-induced electrosensitization, PLoS One 6 (2011) e17100.
[68] C. Poignard, A. Silve, F. Campion, L.M. Mir, O. Saut, L. Schwartz, Ion fluxes, transmembrane potential, and osmotic stabilization: a new dynamic electrophysiological model for eukaryotic cells, Eur. Biophys. J. 40 (2011) 235–246.
[69] A.A. Gurtovenko, I. Vattulainen, Ion leakage through transient water pores in protein-free lipid membranes driven by transmembrane ionic charge imbalance, Biophys. J. 92 (2007) 1878–1890.
[70] S. Kalinowski, G. Ibron, K. Bryl, Z. Figaszewski, Chronopotentiometric studies of electroporation of bilayer lipid membranes, Biochim. Biophys. Acta 1369 (1998) 204–212.